Draft version December 1, 2025
Typeset using LaTeX default style in AASTeX631

BSN: The First Multiband Light Curve Analysis of the W UMa-type Contact Binary System EM Tucanae

Sepideh Houshiar,[1,*] Atila Poro,[2,3] Abbas Abedini,[1] and Eduardo Fernández Lajús[4]

[1] Department of Physics, University of Qom, Qom, Iran
[2] LUX, Observatoire de Paris, CNRS, PSL, 61 Avenue de l'Observatoire, 75014 Paris, France
[3] BSN Project; Astronomy Department of the Raderon AI Lab., BC., Burnaby, Canada
[4] Instituto de Astrofísica de La Plata (CCT La Plata-CONICET-UNLP), La Plata, Argentina

ABSTRACT

We present a comprehensive photometric light curve and orbital period analysis of the W UMa-type contact binary EM Tuc. The O-C analysis constructed from all available eclipse timings exhibits a clear upward parabolic trend, indicating a continuous increase in the orbital period at a rate of $dP/dt = (1.401 \pm 0.042) \times 10^{-7}\,\mathrm{d\,yr^{-1}}$. This behavior is consistent with mass transfer from the less massive to the more massive star in the system, and the corresponding mass-transfer rate is estimated to be $\dot{M} = -(4.62 \pm 1.54) \times 10^{-8}\,M_{\odot}\,\mathrm{yr^{-1}}$. Light curve modeling with the PHysics Of Eclipsing BinariEs (PHOEBE) Python code, refined through MCMC sampling, confirms an overcontact configuration and yields a mass ratio of $q = 3.987$. A cool photospheric starspot on the cooler component is required to reproduce the observed O'Connell asymmetry. Using Gaia DR3 parallax together with the photometric solution, the absolute masses of the components are derived as $M_h = 0.24 \pm 0.05\,M_{\odot}$ and $M_c = 0.97 \pm 0.19\,M_{\odot}$.

Keywords: binaries: eclipsing - methods: observational - stars: individual (EM Tuc)

1. INTRODUCTION

W Ursae Majoris (W UMa) systems form a well-known subclass of eclipsing binaries in which both components fill their Roche lobes and exist in a state of geometric contact (Paczyński 1971[1]). The two stars share a common convective envelope (Lucy 1968[2]), allowing continuous transfer of mass and energy between them. As a result, although the components may differ in mass, structure, and evolutionary status, they maintain nearly identical surface temperatures, which is one of the defining observational characteristics of contact binaries. The orbital periods of W UMa systems are typically short, and most systems exhibit periods in the range of approximately 0.2–0.6 days (Pribulla, Kreiner, & Tremko 2003; Dryomova & Svechnikov 2006; Latković, Čeki, & Lazarević 2021; Poro et al. 2024[3,4,5,6]). A prominent observational feature in many contact binaries is the O'Connell effect, in which the two maxima outside of eclipse in the light curve have unequal brightness (O'Connell 1951; Applegate 1992[7,8]). This asymmetry is commonly attributed to surface inhomogeneities such as starspots, enhanced magnetic activity, or mass-transfer streams impacting one of the components.

Mass and energy exchange play a central role in the dynamics and long-term evolution of contact systems. Depending on the direction and rate of mass transfer, the binary may experience angular momentum loss, thermal relaxation oscillations, or transitions between contact, semi-detached, and near-contact phases. Despite decades of investigation, many aspects of their structural configuration, mass transfer behavior, angular momentum evolution, and eventual merger pathways remain open questions (Zhou et al. 2016[9]).

Recent large-scale surveys such as Gaia and TESS have significantly increased the number of known contact binaries (Latković, Čeki, & Lazarević 2021[5]), yet many systems still lack precise determinations of their fundamental parameters. Accurate measurements of the mass ratio, fillout factor, temperature difference, and fillout factor are critical for distinguishing between stable thermal-contact configurations and systems that are undergoing mass ratio

* sepideh.hoshyar@gmail.com

reversal or evolving toward merger (Gazeas & Stępień 2008; Kouzuma 2018[10,11]). Therefore, detailed investigation of individual W UMa systems remains essential for refining empirical correlations, improving population statistics, and testing evolutionary models that predict whether a given system will remain in contact, transition into a semi-detached state, or eventually coalesce into a rapidly rotating single star.

In this work, we perform a detailed light curve analysis of the W UMa-type contact system EM Tuc in order to obtain its physical and orbital parameters and to better constrain its evolutionary configuration. EM Tuc was first reported by Avery & Sievers (1968)[12] as a variable object. The target is located in the southern hemisphere at RA. : 0.506924° and DEC. : −66.88863° according to Gaia DR3 (Gaia Collaboration et al. 2023[13]). EM Tuc has been classified as a contact binary in several major variable star catalogs, including the Variable Star Index (VSX[1]), the All-Sky Automated Survey for Supernovae (ASAS-SN, Jayasinghe et al. 2018[14]), and Zwicky Transient Facility (ZTF, Sánchez-Sáez et al. 2023[15]), based on consistent photometric evidence indicating an overcontact configuration. The orbital period listed in the VSX database is $P = 0.3265745$ d, which places EM Tuc among short-period contact binaries. The system reaches a reported maximum brightness of approximately $V \approx 12.05$ mag, as reported in the VSX database.

This work continues the observational and analytical approach of the BSN[2] project, focusing on photometric analysis of eclipsing binaries. In this study, we carry out a detailed investigation of the orbital period variations, perform a photometric light-curve analysis, and determine the absolute parameters of the target contact binary EM Tuc.

2. OBSERVATIONS AND DATA REDUCTION

Photometric observations of EM Tuc were conducted on 20 September 2023, during which 1053 images were obtained in a single night. The observations were carried out with the 2.15-meter Jorge Sahade (JS) telescope at the Complejo Astronómico El Leoncito (CASLEO) Observatory, San Juan, Argentina (coordinates: 31°48′ S, 69°18′ W; altitude 2552 m). A VersArray 2048B cryogenic CCD camera (Roper Scientific, Princeton Instruments) was used, along with standard BVR_cI_c filters. All frames were binned 5×5 pixels. The exposure times were 25 s for B, 12 s for V, 12 s for R_c, and 7 s for I_c filters.

Standard CCD reductions, including bias subtraction and flat-field correction, were performed on all images. Aperture photometry was carried out using the APPHOT package in IRAF (Tody 1986[16]). To correct for airmass effects, a Python routine based on the Astropy package (Astropy Collaboration et al. 2013[17]) and following the method of Hiltner (1962)[18] was applied. The fluxes were then normalized using AstroImageJ (Collins et al. 2017[19]).

Time-series photometric data for this study were acquired by the Transiting Exoplanet Survey Satellite (TESS), which is equipped with four wide-field cameras to continuously monitor sections of the sky for exoplanet detection. EM Tuc (TIC 412063998) was observed in sectors 27, 28, and 68, with exposure times of 600 s, 600 s, and 200 s, respectively, and a monitoring duration of approximately 27.4 days per sector. Photometric measurements in the broad "TESS:T" band (600–1000 nm) were retrieved from the Mikulski Archive for Space Telescopes (MAST[3]). Light-curve processing and data reduction were carried out using the Lightkurve package, applying detrending methods consistent with the Science Processing Operations Center (SPOC) pipeline.

3. ORBITAL PERIOD VARIATIONS

A detailed investigation of EM Tuc required a comprehensive collection of eclipse timing measurements, combining archival photometric survey data and our observations. Orbital period variations of this system were examined using these measurements. Published times of minima were collected from various databases and the literature to complement the dataset. Eclipse timings were also directly extracted from the TESS time series, providing consistent and extended coverage where ground-based observations were limited.

This study's multi-filter photometric observations provided additional eclipse timings, enhancing the temporal coverage and strengthening the reliability of the period variation study alongside the data collected from archival surveys. Consistency among all timing measurements was ensured by converting Heliocentric Julian Dates (HJD) into

[1] https://vsx.aavso.org/
[2] https://bsnp.info/
[3] https://mast.stsci.edu/portal/Mashup/Clients/Mast/Portal.html

Table 1. Times of light minimum of ground-based observations.

Min.(BJD_{TDB})	Error	Epoch	O-C	Reference
2454290.63344		0	0	VSX
2455004.52275	0.00200	2186	-0.0025	Paschke (2009)
2455004.68675	0.00300	2186.5	-0.0018	Paschke (2009)
2460208.65139	0.00120	18121.5	-0.0019	This study
2460208.81419	0.00112	18122	-0.0023	This study

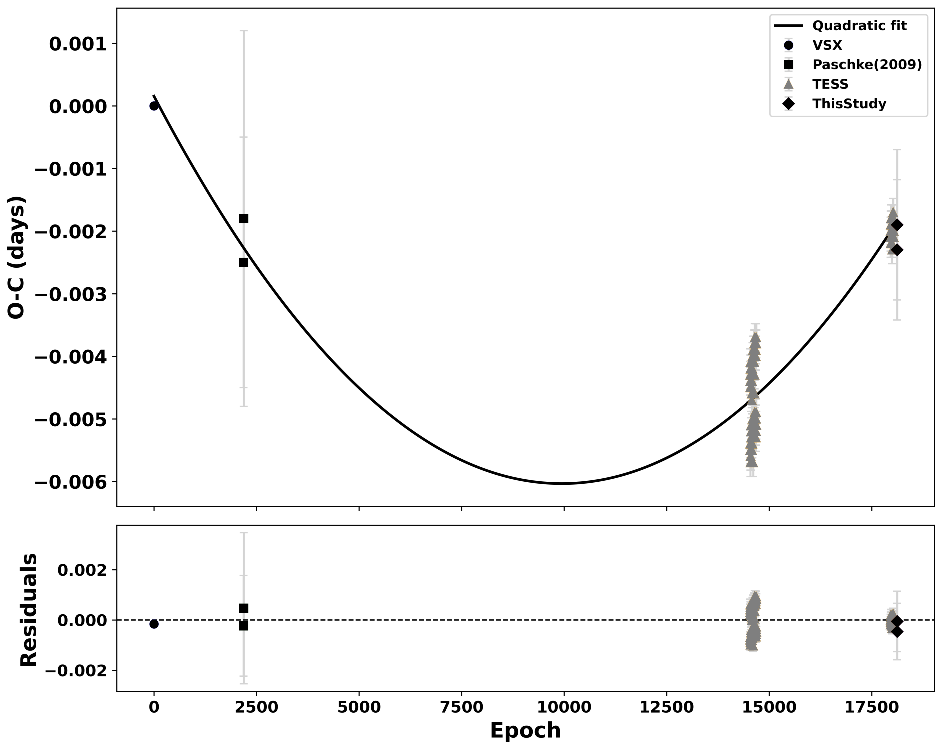

Figure 1. The O-C diagram of the EM Tuc contact binary.

Barycentric Julian Dates in Barycentric Dynamical Time (BJD_{TDB}; Eastman, Siverd, & Gaudi 2010[20]). An online calculator[4] was employed to perform the conversion. Eclipse timings are provided in Tables 1 and A1.

The light elements from the VSX database were adopted as the reference ephemeris for computing the epoch and O–C values (Equation 1).

$$BJD_{TDB}(Min.I) = 2454290.63344 + 0.3265745 \times E. \quad (1)$$

where E is the number of cycles.

Using the gathered eclipse timing measurements and the reference ephemeris, a new linear ephemeris was derived for the system, providing an updated basis for computing epochs and O–C values (Equation 2).

$$BJD_{TDB}(Min.I) = 2454290.63359(37) + 0.32657325(5) \times E. \quad (2)$$

The O–C diagram of EM Tuc is shown in Figure 1, together with the corresponding fit residuals. The diagram exhibits an upward parabolic trend, revealing a continuous increase in the orbital period of the system. The derived

[4] https://astroutils.astronomy.osu.edu/time/hjd2bjd.html

period change rate is $dP/dt = (1.401 \pm 0.0421) \times 10^{-7}$ d yr^{-1}. Since the hotter component is the less massive star and the cooler component is the more massive one, this positive period derivative indicates that mass is being transferred from the hotter to the cooler component.

4. PARAMETER ESTIMATIONS

4.1. *Light Curve Solution*

Light curve modeling of the EM Tuc system was performed with PHOEBE v2.4.9 in combination with an MCMC approach (Prša et al. 2016; Conroy et al. 2020[22,23]). Based on the overall morphology of the observed light variation and the short orbital period, the configuration of a contact binary was adopted for the solution. The observational times were converted to orbital phase using the updated ephemeris determined in this work (Section 3). The gravity darkening coefficients and bolometric albedos were fixed to $g_1 = g_2 = 0.32$ (Lucy 1967[24]) and $A_1 = A_2 = 0.5$ (Ruciński 1969[25]). Limb-darkening was considered as a free parameter in the process, and stellar atmospheres were represented using the Castelli & Kurucz (2004)[26] study. The adopted initial effective temperature of the hotter component follows the value reported in Gaia DR3 (Poro et al. 2025[27]). The effective temperature of the cooler star was estimated based on the relative depths of the primary and secondary eclipses in the observed light curve. The mass ratio (q) is a critical parameter in modeling contact binaries, so a q-search was conducted in PHOEBE (Terrell & Wilson 2005[28]). A wide interval of mass ratios, spanning from 0.1 to 20, was first examined for each system. After identifying the region that provided a closer agreement with the observations, the search range was gradually reduced (Figure 2).

Asymmetries between the two light-curve maxima are frequently seen in contact binaries, and such behavior is also evident in our target. This effect is generally interpreted as the result of starspots associated with magnetic activity, commonly referred to as the O'Connell effect (O'Connell 1951[7]).

The light curves of the system were modeled without including a third-light term (l_3). No signs of contamination from neighboring sources were identified, and there is currently no strong indication of a third-light contribution.

After determining the most plausible values for main model parameters, they were refined using the PHOEBE's built-in optimization routine. The photometric analysis was further validated using the BSN application (Paki, Poro, & Moosavi Rowzati 2025[29]). The initial version of this application, which runs on Microsoft Windows operating system, offers high processing speed and makes the determination of starspot coordinates considerably easier for the user. Then, the output parameter estimates and their uncertainties were obtained using the Markov Chain Monte Carlo (MCMC) approach implemented with the emcee Python package (Foreman-Mackey et al. 2013[30]). In this analysis, 96 walkers were initialized around the best-fit solution from the previous optimization step. Each walker was evolved for 1000 iterations, with the first 200 iterations discarded as burn-in to ensure convergence. The resulting posterior distributions were used to determine the median values as the parameter estimates and the 16th and 84th percentiles as their corresponding uncertainties.

Figure 3 presents the corner plots for the EM Tuc system, illustrating the distributions and correlations of parameters obtained from the MCMC analysis. The final results of the light curve analysis, including starspot characteristics (longitude, colatitude, radius, $T_{\rm spot}/T_{\rm star}$), are summarized in Table 2. The observed and synthetic light curves in different filters are displayed in Figure 4. Three-dimensional representations of the binary systems, constructed from the final model parameters, are presented in Figure 5 at orbital phases 0, 0.25, 0.5, and 0.75, respectively.

4.2. *Absolute Parameters*

The absolute parameters of EM Tuc were derived by using the Gaia DR3 parallax with the photometric solution. Our approach follows the methodology of Poro et al. (2022)[31], where the physical properties of both components can be determined once several observational and model-dependent quantities are known. These include the orbital period (P), the mean fractional radii ($r_{mean1,2}$), the effective temperatures ($T_{1,2}$), the bolometric corrections ($BC_{1,2}$), the fractional light contributions ($l_{1,2}/l_{tot}$), the interstellar extinction (A_v), the system's maximum brightness (V_{max}), and the distance (d) from Gaia DR3. Based on these quantities, we derived the absolute visual magnitudes of the system and its individual components, followed by their bolometric magnitudes, luminosities, radii, and masses. The orbital separation was calculated as the average of the two separately determined values, a_1 and a_2. This method is valid only when a_1 and a_2 closely agree, ensuring the internal consistency of the solution.

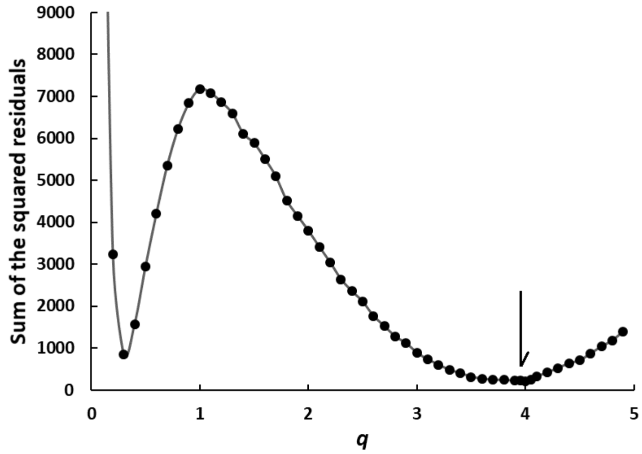

Figure 2. The sum of squared residuals as a function of mass ratio. The black arrow indicates the estimated mass ratio in the q-search.

Table 2. Results of light curve solution.

Parameter	Result	Parameter	Result
T_h (K)	5901^{+4}_{-4}	$r_{(mean)_h}$	0.275 ± 0.023
T_c (K)	5563^{+5}_{-5}	$r_{(mean)_c}$	0.510 ± 0.020
q	$3.987^{+0.016}_{-0.011}$	$Col^{\circ}_{\rm spot}$	110(1)
i°	$80.88^{+0.06}_{-0.05}$	$Long^{\circ}_{\rm spot}$	272(2)
f	$0.138^{+0.006}_{-0.005}$	$Radius^{\circ}_{\rm spot}$	15(1)
$\Omega_h = \Omega_c$	7.808 ± 0.315	$T_{\rm spot}/T_{\rm star}$	0.78(1)
l_h/l_{tot}	$0.262^{+0.001}_{-0.001}$	Spot Component	Cooler star
l_c/l_{tot}	0.738 ± 0.005	MaxI-MaxII (Flux)	0.036

The maximum brightness of EM Tuc was measured as $V_{max} = 12.17 \pm 0.10$ from our photometric light curve. The interstellar extinction was determined as $A_V = 0.060 \pm 0.001$ following the three-dimensional dust maps from Green et al. (2019)[32], and the system distance was taken as $d = 335(7)$ pc from Gaia DR3. Bolometric corrections of $BC_{1,2}$ were assigned according to the calibration of Flower (1996)[33].

The luminosities and surface gravities were computed using the following commonly adopted relations:

$$M_{\rm bol} - M_{\rm bol,\odot} = -2.5 \log \left(\frac{L}{L_{\odot}} \right), \tag{3}$$

$$g = G_{\odot} \frac{M}{R^2}, \tag{4}$$

where solar bolometric magnitude of $M_{\rm bol\odot} = 4.73$ mag (Torres 2010[34]), and $G_{\odot}$ is the solar gravitational constant.

The resulting physical parameters derived using this parallax-based method are summarized in Table 3.

5. DISCUSSION AND CONCLUSION

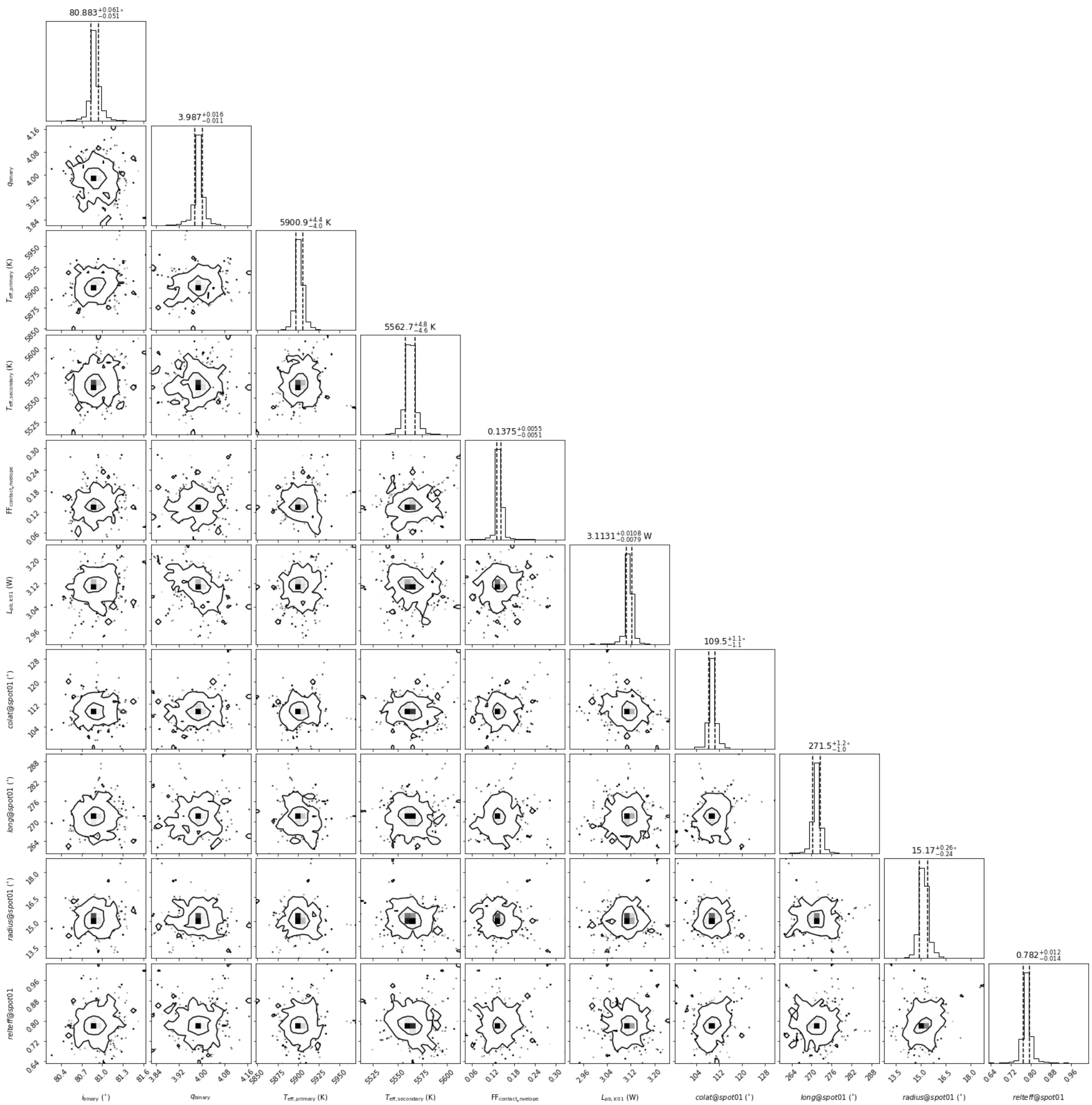

Figure 3. The corner plots of EM Tuc determined by MCMC modeling. The parameters used in the MCMC procedure, presented in the corner plot, include: i, q, T_1, T_2, f, l_1, and four starspot parameters, respectively.

We carried out ground-based multiband photometric observations of the southern eclipsing binary EM Tuc using the B, V, R_c, and I_c filters. Combining the ground-based data with TESS observations allowed us to perform an in-depth light curve analysis and to study the orbital period variations of the system.

Based on the analysis of the O-C diagram and the quadratic fit, the mass transfer rate in the EM Tuc system has been estimated. In this system, mass is transferred from the less massive component to the more massive one, and

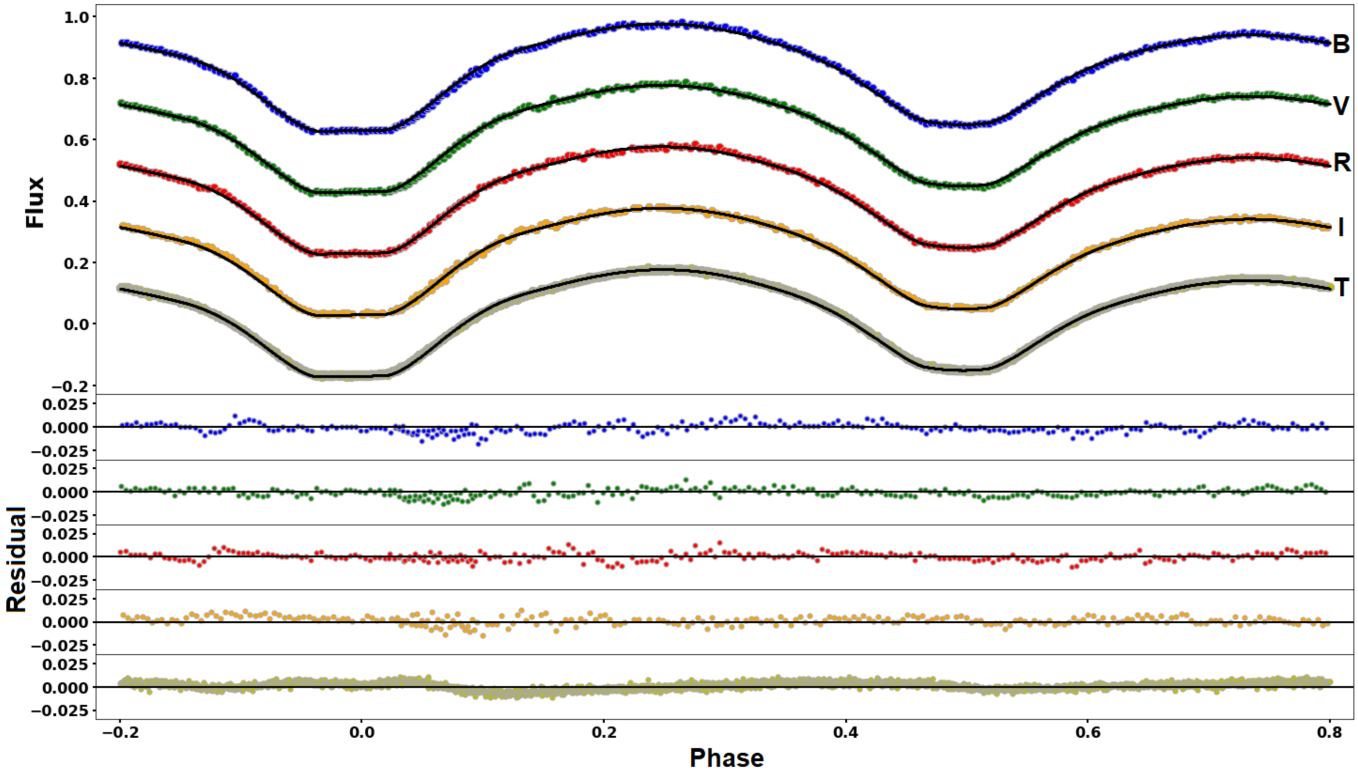

Figure 4. Ground- and space-based photometric light curves together with synthetic model.

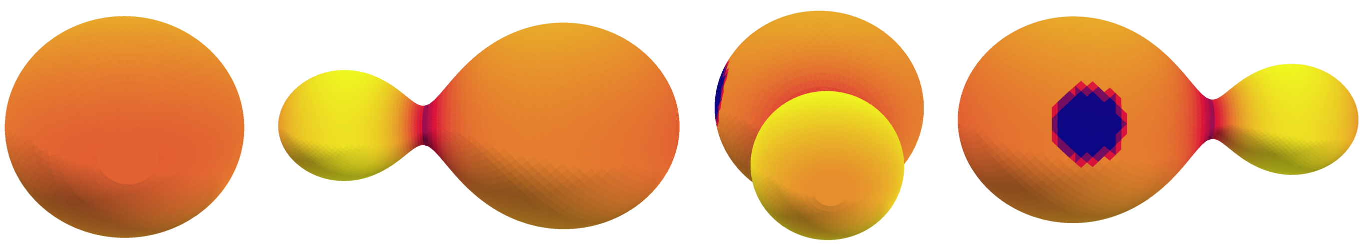

Figure 5. 3D view of the target system stars.

Table 3. Estimation of absolute parameters.

Parameter	Hotter Star	Colder Star
$M(M_\odot)$	0.24 ± 0.05	0.97 ± 0.19
$R(R_\odot)$	0.58 ± 0.04	1.09 ± 0.08
$L(L_\odot)$	0.37 ± 0.05	1.03 ± 0.14
M_{bol}(mag.)	5.83 ± 0.14	4.71 ± 0.14
$log(g)$(cgs)	4.30 ± 0.14	4.35 ± 0.15
$a(R_\odot)$	2.13 ± 0.14	

this process can be described by the Equation 5:

$$\dot{M}_1 = -\frac{(dP/P)}{3\left(\frac{1}{M_1} - \frac{1}{M_2}\right)}. \tag{5}$$

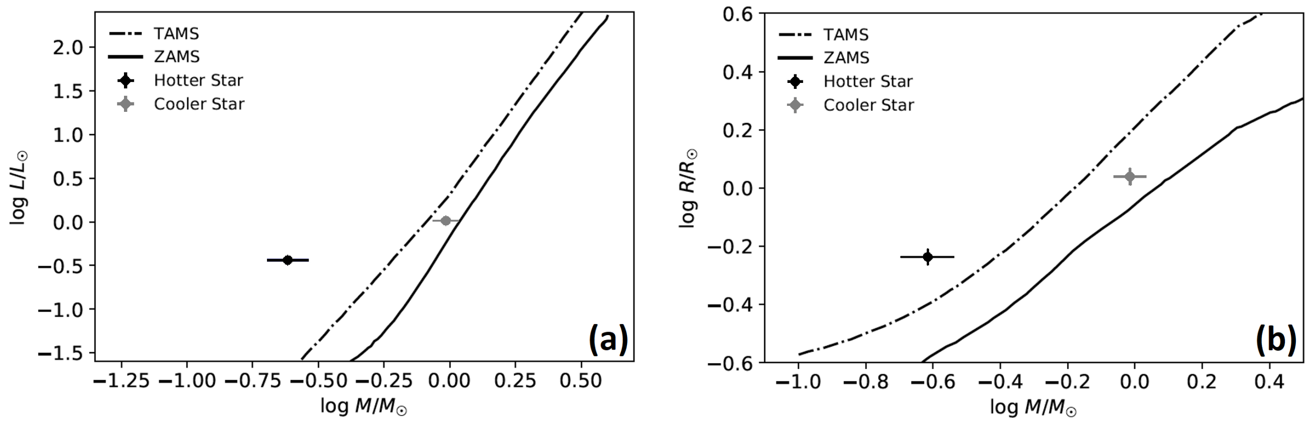

Figure 6. M-L and M-R diagrams of the contact system EM Tuc, showing the evolutionary stages of the components with respect to ZAMS and TAMS.

The resulting mass transfer rate is $-4.618 \pm 1.537 \times 10^{-8}\ M_\odot\,\mathrm{yr}^{-1}$, indicating that mass is being transferred from the less massive component to the more massive one, which highlights that the system is currently in an active phase of mass exchange.

This mass transfer rate, which lies within the order of $10^{-8}\ M_\odot\,\mathrm{yr}^{-1}$, has significant implications for the physical and evolutionary properties of EM Tuc. The increase in mass of the more massive star and the corresponding decrease of the less massive star lead to changes in the mass ratio and orbital dynamics, potentially affecting the degree of contact and the structural configuration of the components. Furthermore, mass transfer directly influences the stellar internal structure and surface energy distribution, as hydrostatic equilibrium and surface temperature respond to the changing masses, which may also impact the luminosities and radii of both stars. Overall, this process plays a crucial role in the future evolution of the system and is consistent with the characteristics of short-period contact binaries with low mass ratios.

We modeled the light curve using the PHOEBE Python package, and the final parameter values along with their uncertainties were determined through the MCMC approach. The temperature difference between the two stars is 338 K. Based on these temperatures and the spectral classifications provided by Eker et al. (2018)[35], the hotter component corresponds to a G2 spectral type, while the cooler one is classified as G8. The light-curve modeling of EM Tuc also required including a cool starspot on the surface of the cooler component to achieve an acceptable fit.

Contact binary systems can be divided into three groups depending on their fillout factor: deep systems with $f \geq 50\%$, medium systems with $25\% \leq f < 50\%$, and shallow systems with $f < 25\%$ (Li et al. 2022[36]). According to the light curve modeling, EM Tuc belongs to the shallow class.

The absolute parameters of EM Tuc were estimated using the Gaia DR3 parallax. In this method, the paths of the primary and secondary stars are treated independently, giving semi-major axes $a_1(R_\odot)$ and $a_2(R_\odot)$ for each component. The resulting values are in good agreement, with a small difference of $\Delta a = |a_2 - a_1| = 0.009$, supporting the reliability of the approach. This Δa further confirms the validity of the light curve solution and the adopted model parameters (Poro et al. 2024, 2025[37,38]).

The evolutionary state of EM Tuc was examined through logarithmic Mass-Radius (M-R) and Mass-Luminosity (M-L) diagrams, based on the absolute parameters derived for the system (Figures 6a,b). In these diagrams, the locations of both components are compared with the Zero-Age Main Sequence (ZAMS) and Terminal-Age Main Sequence (TAMS) reference tracks from Girardi et al. (2000)[39], allowing us to assess their evolutionary progression along the main sequence. As shown in Figures 6a,b, the less massive component is positioned above the TAMS line, whereas the more massive star lies closer to the ZAMS. This indicates that the two components occupy different evolutionary stages along the main sequence.

In this work, EM Tuc is identified as a W UMa-type contact eclipsing binary through light curve modeling using the derived mass ratio, fillout factor, and orbital inclination, which clearly confirm its contact configuration. According to the classification framework for A- and W-type contact binaries proposed by Binnendijk (1970)[40], and based on the derived component masses and temperatures (Poro et al. 2024[41]), EM Tuc falls into the W-subtype category.

In W-type systems, the hotter component is the less massive star, which is consistent with the physical properties obtained for EM Tuc.

DATA AVAILABILITY

Ground-based observational data used in this study are available from the corresponding author upon reasonable request.

6. ACKNOWLEDGMENTS

We used data from the European Space Agency mission Gaia[5]. This work includes data from the TESS mission observations. The NASA Explorer Program provides funding for the TESS mission.

APPENDIX

The appendix table presents the primary and secondary times of minima for the EM Tuc contact binary system, derived from TESS observations. The average uncertainty in the times of minima is 0.00022.

REFERENCES

[1] Paczyński B., 1971, ARA&A, 9, 183.
[2] Lucy L. B., 1968, ApJ, 151, 1123.
[3] Pribulla T., Kreiner J. M., Tremko J., 2003, CoSka, 33, 38.
[4] Dryomova G. N., Svechnikov M. A., 2006, Ap, 49, 358.
[5] Latković O., Čeki A., Lazarević S., 2021, ApJS, 254, 10.
[6] Poro A., Paki E., Alizadehsabegh A., et al., 2024, RAA, 24, 015002.
[7] O'Connell D. J. K., 1951, PRCO, 2, 85.
[8] Applegate J. H., 1992, ApJ, 385, 621.
[9] Zhou X., Qian S.-B., Zhang J., et al., 2016, ApJ, 817, 133.
[10] Gazeas K., Stępień K., 2008, MNRAS, 390, 1577.
[11] Kouzuma S., 2018, PASJ, 70, 90.
[12] Avery R., Sievers J., 1968, BamVe, 7, 76
[13] Gaia Collaboration, Vallenari A., Brown A. G. A., Prusti T., et al., 2023, A&A, 674, A1.
[14] Jayasinghe T., Kochanek C. S., Stanek K. Z., et al., 2018, MNRAS, 477, 3145.
[15] Sánchez-Sáez P., Arredondo J., Bayo A., et al., 2023, A&A, 675, A195.
[16] Tody D., 1986, SPIE, 627, 733.
[17] Astropy Collaboration, Robitaille T. P., Tollerud E. J., Greenfield P., et al., 2013, A&A, 558, A33.
[18] Hiltner W. A., 1962, aste.book.
[19] Collins K. A., Kielkopf J. F., Stassun K. G., Hessman F. V., 2017, AJ, 153, 77.
[20] Eastman J., Siverd R., Gaudi B. S., 2010, PASP, 122, 935.
[21] Paschke A., 2009, OEJV, 0116, 1.
[22] Prša A., Conroy K. E., Horvat M., et al., 2016, ApJS, 227, 29.
[23] Conroy K. E., Kochoska A., Hey D., et al., 2020, ApJS, 250, 34.
[24] Lucy L. B., 1967, ZA, 65, 89.

[5] http://www.cosmos.esa.int/gaia

Table A1. Times of Minima extracted from the TESS data.

Min.(BJD_{TDB})	Epoch	O-C	Min.(BJD_{TDB})	Epoch	O-C	Min.(BJD_{TDB})	Epoch	O-C
2459036.40860	14532	-0.0055	2459047.51251	14566	-0.0051	2459059.76011	14603.5	-0.0040
2459036.57286	14532.5	-0.0045	2459047.67658	14566.5	-0.0043	2459059.92239	14604	-0.0051
2459036.73525	14533	-0.0054	2459047.83901	14567	-0.0052	2459060.08671	14604.5	-0.0040
2459036.89952	14533.5	-0.0044	2459048.00328	14567.5	-0.0042	2459060.24885	14605	-0.0052
2459037.06181	14534	-0.0054	2459049.30916	14571.5	-0.0046	2459060.41321	14605.5	-0.0041
2459037.22617	14534.5	-0.0043	2459049.47168	14572	-0.0054	2459060.57537	14606	-0.0052
2459037.38834	14535	-0.0055	2459049.63572	14572.5	-0.0046	2459062.04587	14610.5	-0.0043
2459037.55267	14535.5	-0.0044	2459049.79826	14573	-0.0054	2459062.20780	14611	-0.0057
2459037.71496	14536	-0.0054	2459049.96240	14573.5	-0.0045	2459062.53478	14612	-0.0053
2459037.87931	14536.5	-0.0044	2459050.12493	14574	-0.0053	2459062.69918	14612.5	-0.0041
2459038.04144	14537	-0.0055	2459050.28880	14574.5	-0.0047	2459062.86136	14613	-0.0053
2459038.20609	14537.5	-0.0041	2459050.45136	14575	-0.0054	2459063.02602	14613.5	-0.0039
2459038.36799	14538	-0.0055	2459050.61539	14575.5	-0.0047	2459063.18796	14614	-0.0052
2459038.53267	14538.5	-0.0041	2459050.77805	14576	-0.0053	2459063.35245	14614.5	-0.0040
2459038.69450	14539	-0.0056	2459050.94200	14576.5	-0.0046	2459063.51450	14615	-0.0053
2459038.85924	14539.5	-0.0041	2459051.10457	14577	-0.0054	2459063.67908	14615.5	-0.0040
2459039.02111	14540	-0.0056	2459051.26854	14577.5	-0.0047	2459063.84110	14616	-0.0052
2459039.18575	14540.5	-0.0042	2459051.43106	14578	-0.0054	2459064.00568	14616.5	-0.0039
2459039.34784	14541	-0.0054	2459051.59520	14578.5	-0.0046	2459064.16760	14617	-0.0053
2459039.51224	14541.5	-0.0043	2459051.75770	14579	-0.0054	2459064.33220	14617.5	-0.0040
2459039.67411	14542	-0.0057	2459051.92190	14579.5	-0.0045	2459064.49419	14618	-0.0053
2459039.83886	14542.5	-0.0042	2459052.08421	14580	-0.0054	2459064.65882	14618.5	-0.0040
2459040.00095	14543	-0.0054	2459052.24852	14580.5	-0.0044	2459064.82091	14619	-0.0051
2459040.16546	14543.5	-0.0042	2459052.41087	14581	-0.0054	2459064.98538	14619.5	-0.0040
2459040.32747	14544	-0.0055	2459052.57509	14581.5	-0.0044	2459065.14754	14620	-0.0051
2459040.49211	14544.5	-0.0041	2459052.73747	14582	-0.0053	2459065.31197	14620.5	-0.0040
2459040.65407	14545	-0.0055	2459052.90171	14582.5	-0.0044	2459065.47402	14621	-0.0052
2459040.81860	14545.5	-0.0042	2459053.06389	14583	-0.0055	2459065.63850	14621.5	-0.0040
2459040.98056	14546	-0.0056	2459053.22822	14583.5	-0.0044	2459065.80078	14622	-0.0050
2459041.14517	14546.5	-0.0042	2459053.39056	14584	-0.0054	2459065.96519	14622.5	-0.0039
2459041.30712	14547	-0.0056	2459053.55487	14584.5	-0.0044	2459066.12728	14623	-0.0051
2459041.47185	14547.5	-0.0041	2459053.71713	14585	-0.0054	2459066.29164	14623.5	-0.0040
2459041.63370	14548	-0.0056	2459053.88153	14585.5	-0.0043	2459066.45380	14624	-0.0051
2459041.79835	14548.5	-0.0042	2459054.04366	14586	-0.0054	2459066.61828	14624.5	-0.0039
2459041.96048	14549	-0.0054	2459054.20809	14586.5	-0.0043	2459066.78043	14625	-0.0051
2459042.12480	14549.5	-0.0043	2459054.37031	14587	-0.0054	2459066.94488	14625.5	-0.0039
2459042.28687	14550	-0.0055	2459054.53470	14587.5	-0.0043	2459067.10688	14626	-0.0052
2459042.45148	14550.5	-0.0042	2459054.69684	14588	-0.0054	2459067.27148	14626.5	-0.0039
2459042.61344	14551	-0.0056	2459054.86136	14588.5	-0.0042	2459067.43359	14627	-0.0051
2459042.77801	14551.5	-0.0043	2459055.02351	14589	-0.0053	2459067.59804	14627.5	-0.0039
2459042.94005	14552	-0.0055	2459055.18790	14589.5	-0.0042	2459067.76011	14628	-0.0051
2459043.10448	14552.5	-0.0044	2459055.34997	14590	-0.0054	2459067.92469	14628.5	-0.0038
2459043.26664	14553	-0.0055	2459055.51443	14590.5	-0.0043	2459068.08664	14629	-0.0052
2459043.43106	14553.5	-0.0044	2459055.67664	14591	-0.0053	2459068.25120	14629.5	-0.0039
2459043.59327	14554	-0.0054	2459055.84122	14591.5	-0.0040	2459068.41321	14630	-0.0052
2459043.75770	14554.5	-0.0043	2459056.00332	14592	-0.0052	2459068.57769	14630.5	-0.0040
2459043.91983	14555	-0.0055	2459056.16781	14592.5	-0.0040	2459068.73983	14631	-0.0051
2459044.08421	14555.5	-0.0044	2459056.33014	14593	-0.0050	2459068.90437	14631.5	-0.0039
2459044.24666	14556	-0.0052	2459056.49442	14593.5	-0.0040	2459069.06633	14632	-0.0052
2459044.41070	14556.5	-0.0045	2459056.65671	14594	-0.0050	2459069.23091	14632.5	-0.0039
2459044.57329	14557	-0.0051	2459056.82095	14594.5	-0.0040	2459069.39293	14633	-0.0052
2459044.73761	14557.5	-0.0041	2459056.98321	14595	-0.0051	2459069.55737	14633.5	-0.0040
2459044.89976	14558	-0.0053	2459057.14750	14595.5	-0.0041	2459069.71949	14634	-0.0052
2459045.06406	14558.5	-0.0042	2459057.30988	14596	-0.0050	2459069.88389	14634.5	-0.0041
2459045.22631	14559	-0.0053	2459057.47402	14596.5	-0.0041	2459070.04602	14635	-0.0052
2459045.39069	14559.5	-0.0042	2459057.63631	14597	-0.0051	2459070.21051	14635.5	-0.0040
2459045.55294	14560	-0.0052	2459057.80058	14597.5	-0.0041	2459070.37263	14636	-0.0052
2459045.71712	14560.5	-0.0043	2459057.96293	14598	-0.0051	2459070.53699	14636.5	-0.0041
2459045.87950	14561	-0.0052	2459058.12723	14598.5	-0.0041	2459070.69928	14637	-0.0051
2459046.04382	14561.5	-0.0042	2459058.28952	14599	-0.0050	2459070.86359	14637.5	-0.0041
2459046.20610	14562	-0.0052	2459058.45387	14599.5	-0.0040	2459071.02595	14638	-0.0050
2459046.37013	14562.5	-0.0045	2459058.61605	14600	-0.0051	2459071.19016	14638.5	-0.0041
2459046.53265	14563	-0.0052	2459058.78040	14600.5	-0.0040	2459071.35256	14639	-0.0050
2459046.69675	14563.5	-0.0044	2459058.94266	14601	-0.0051	2459071.51678	14639.5	-0.0041
2459046.85927	14564	-0.0052	2459059.10706	14601.5	-0.0039	2459071.67927	14640	-0.0049
2459047.02324	14564.5	-0.0045	2459059.26918	14602	-0.0051	2459071.84357	14640.5	-0.0038
2459047.18586	14565	-0.0052	2459059.43346	14602.5	-0.0041	2459072.00581	14641	-0.0049
2459047.34988	14565.5	-0.0044	2459059.59577	14603	-0.0051	2459072.17008	14641.5	-0.0039

Table A1. Continued.

Min.(BJD_{TDB})	Epoch	O-C	Min.(BJD_{TDB})	Epoch	O-C	Min.(BJD_{TDB})	Epoch	O-C
2459072.33233	14642	-0.0049	2459082.78254	14674	-0.0051	2460164.23698	17985.5	-0.0021
2459072.49659	14642.5	-0.0040	2459082.94703	14674.5	-0.0039	2460164.56363	17986.5	-0.0021
2459072.65899	14643	-0.0049	2459083.10902	14675	-0.0052	2460164.89022	17987.5	-0.0020
2459072.82315	14643.5	-0.0040	2459083.27370	14675.5	-0.0038	2460165.21678	17988.5	-0.0021
2459072.98548	14644	-0.0049	2459083.43550	14676	-0.0053	2460165.54334	17989.5	-0.0021
2459073.14997	14644.5	-0.0037	2459083.60030	14676.5	-0.0038	2460165.87001	17990.5	-0.0020
2459073.31185	14645	-0.0051	2459083.76217	14677	-0.0052	2460166.19653	17991.5	-0.0020
2459073.47601	14645.5	-0.0043	2459083.92693	14677.5	-0.0037	2460166.52305	17992.5	-0.0021
2459073.63896	14646	-0.0046	2459084.08861	14678	-0.0053	2460166.84959	17993.5	-0.0021
2459073.80296	14646.5	-0.0039	2459084.25346	14678.5	-0.0038	2460167.17620	17994.5	-0.0021
2459075.27123	14651	-0.0052	2459084.41554	14679	-0.0050	2460167.50256	17995.5	-0.0023
2459075.43586	14651.5	-0.0039	2459084.58016	14679.5	-0.0037	2460167.82922	17996.5	-0.0022
2459075.59787	14652	-0.0051	2459084.74191	14680	-0.0052	2460168.15588	17997.5	-0.0021
2459075.76236	14652.5	-0.0039	2459084.90668	14680.5	-0.0037	2460168.80909	17999.5	-0.0021
2459076.25083	14654	-0.0053	2459085.06871	14681	-0.0050	2460169.13562	18000.5	-0.0021
2459076.41569	14654.5	-0.0038	2459085.23325	14681.5	-0.0037	2460169.46212	18001.5	-0.0022
2459076.57781	14655	-0.0049	2459085.39521	14682	-0.0050	2460169.78880	18002.5	-0.0021
2459076.74218	14655.5	-0.0038	2459085.55980	14682.5	-0.0037	2460170.11539	18003.5	-0.0021
2459076.90435	14656	-0.0050	2459085.72188	14683	-0.0049	2460170.44204	18004.5	-0.0020
2459077.06879	14656.5	-0.0038	2459086.04835	14684	-0.0051	2460170.76852	18005.5	-0.0021
2459077.23066	14657	-0.0052	2459086.21292	14684.5	-0.0038	2460171.09507	18006.5	-0.0021
2459077.39542	14657.5	-0.0038	2459086.37489	14685	-0.0051	2460171.42165	18007.5	-0.0021
2459077.55731	14658	-0.0052	2459086.53958	14685.5	-0.0037	2460171.74831	18008.5	-0.0020
2459077.72191	14658.5	-0.0038	2459086.70146	14686	-0.0051	2460172.07501	18009.5	-0.0019
2459077.88391	14659	-0.0051	2459086.86604	14686.5	-0.0038	2460172.40160	18010.5	-0.0019
2459078.04854	14659.5	-0.0038	2459087.02804	14687	-0.0051	2460172.72809	18011.5	-0.0020
2459078.21044	14660	-0.0052	2460154.76623	17956.5	-0.0022	2460173.05475	18012.5	-0.0019
2459078.37507	14660.5	-0.0038	2460155.09292	17957.5	-0.0021	2460173.38129	18013.5	-0.0019
2459078.53691	14661	-0.0053	2460155.41962	17958.5	-0.0020	2460173.70797	18014.5	-0.0018
2459078.70162	14661.5	-0.0039	2460155.74607	17959.5	-0.0021	2460174.03453	18015.5	-0.0018
2459078.86355	14662	-0.0052	2460156.07282	17960.5	-0.0019	2460174.36100	18016.5	-0.0019
2459079.02821	14662.5	-0.0038	2460156.39935	17961.5	-0.0020	2460174.68762	18017.5	-0.0019
2459079.19019	14663	-0.0051	2460156.72597	17962.5	-0.0019	2460175.34099	18019.5	-0.0017
2459079.35483	14663.5	-0.0038	2460157.05248	17963.5	-0.0020	2460175.66745	18020.5	-0.0018
2459079.51669	14664	-0.0052	2460157.37922	17964.5	-0.0018	2460175.99406	18021.5	-0.0017
2459079.68132	14664.5	-0.0039	2460157.70571	17965.5	-0.0019	2460176.32062	18022.5	-0.0017
2459079.84329	14665	-0.0052	2460158.03225	17966.5	-0.0019	2460176.64715	18023.5	-0.0018
2459080.00801	14665.5	-0.0038	2460158.35881	17967.5	-0.0020	2460176.97370	18024.5	-0.0018
2459080.16984	14666	-0.0052	2460158.68542	17968.5	-0.0019	2460177.30032	18025.5	-0.0018
2459080.33444	14666.5	-0.0039	2460159.01201	17969.5	-0.0019	2460177.62688	18026.5	-0.0018
2459080.49646	14667	-0.0052	2460159.33858	17970.5	-0.0019	2460177.95336	18027.5	-0.0019
2459080.66098	14667.5	-0.0039	2460159.66523	17971.5	-0.0018	2460178.27996	18028.5	-0.0019
2459080.82301	14668	-0.0052	2460159.99179	17972.5	-0.0019	2460178.60642	18029.5	-0.0020
2459080.98752	14668.5	-0.0040	2460160.31831	17973.5	-0.0019	2460178.93320	18030.5	-0.0018
2459081.14959	14669	-0.0052	2460160.64496	17974.5	-0.0018	2460179.25970	18031.5	-0.0018
2459081.31414	14669.5	-0.0039	2460160.97149	17975.5	-0.0019	2460179.58619	18032.5	-0.0019
2459081.47621	14670	-0.0051	2460161.29813	17976.5	-0.0018	2460179.91276	18033.5	-0.0019
2459081.64060	14670.5	-0.0040	2460161.62455	17977.5	-0.0020	2460180.23924	18034.5	-0.0020
2459081.80275	14671	-0.0052	2460162.27760	17979.5	-0.0021	2460180.56589	18035.5	-0.0019
2459081.96725	14671.5	-0.0040	2460162.60435	17980.5	-0.0019	2460180.89254	18036.5	-0.0019
2459082.12920	14672	-0.0053	2460162.93085	17981.5	-0.0020	2460181.54550	18038.5	-0.0021
2459082.29382	14672.5	-0.0040	2460163.25741	17982.5	-0.0020	2460181.87211	18039.5	-0.0020
2459082.45588	14673	-0.0052	2460163.58398	17983.5	-0.0020			
2459082.62044	14673.5	-0.0039	2460163.91036	17984.5	-0.0022			

[25] Ruciński S. M., 1969, AcA, 19, 245.

[26] Castelli F., Kurucz R. L., 2004, A&A, 419, 725.

[27] Poro A., Li K., Paki E., et al., 2025, MNRAS, 537, 3160.

[28] Terrell D., Wilson R. E., 2005, Ap&SS, 296, 221.

[29] Paki E., Poro A., Moosavi Rowzati M. D., 2025, Galax, 13, 74.

[30] Foreman-Mackey D., Hogg D. W., Lang D., Goodman J., 2013, PASP, 125, 306.

[31] Poro A., Sarabi S., Zamanpour S., et al., 2022, MNRAS, 510, 5315.
[32] Green G. M., Schlafly E., Zucker C., et al., 2019, ApJ, 887, 93.
[33] Flower P. J., 1996, ApJ, 469, 355.
[34] Torres G., 2010, AJ, 140, 1158.
[35] Eker Z., Bakış V., Bilir S., et al., 2018, MNRAS, 479, 5491.
[36] Li K., Gao X., Liu X.-Y., et al., 2022, AJ, 164, 202.
[37] Poro A., Hedayatjoo M., Nastaran M., et al., 2024, NewA, 110, 102227.
[38] Poro A., Jahangiri E., Sarvari E., et al., 2025, MNRAS, 538, 1427.
[39] Girardi L., Bressan A., Bertelli G., Chiosi C., 2000, A&AS, 141, 371.
[40] Binnendijk L., 1970, VA, 12, 217.
[41] Poro A., Baudart S., Nourmohammad M., et al., 2024, RAA, 24, 055001.